Developmental Biology 418 (2016) 75–88

Contents lists available at ScienceDirect

Developmental Biology

journal homepage: www.elsevier.com/locate/developmentalbiology

Original research article

Epiblast-specific loss of HCF-1 leads to failure in anterior-posterior axis specification

Shilpi Minocha [a], Sylvain Bessonnard [b,1], Tzu-Ling Sung [a,2], Catherine Moret [a], Daniel B. Constam [b,*], Winship Herr [a,*]

[a] Center for Integrative Genomics, Génopode, University of Lausanne, 1015 Lausanne, Switzerland
[b] Ecole Polytechnique Fédérale de Lausanne (EPFL) SV ISREC, Station 19, 1015 Lausanne, Switzerland

ARTICLE INFO

Article history:
Received 29 June 2016
Received in revised form
8 August 2016
Accepted 8 August 2016
Available online 9 August 2016

Keywords:
HCF-1/*Hcfc1*
Embryonic lethality
AVE
Gastrulation
Primitive streak
Cell cycle

ABSTRACT

Mammalian Host-Cell Factor 1 (HCF-1), a transcriptional co-regulator, plays important roles during the cell-division cycle in cell culture, embryogenesis as well as adult tissue. In mice, HCF-1 is encoded by the X-chromosome-linked *Hcfc1* gene. Induced *Hcfc1*$^{cKO/+}$ heterozygosity with a conditional knockout (cKO) allele in the epiblast of female embryos leads to a mixture of HCF-1-positive and -deficient cells owing to random X-chromosome inactivation. These embryos survive owing to the replacement of all HCF-1-deficient cells by HCF-1-positive cells during E5.5 to E8.5 of development. In contrast, complete epiblast-specific loss of HCF-1 in male embryos, *Hcfc1*$^{epiKO/Y}$, leads to embryonic lethality. Here, we characterize this lethality. We show that male epiblast-specific loss of *Hcfc1* leads to a developmental arrest at E6.5 with a rapid progressive cell-cycle exit and an associated failure of anterior visceral endoderm migration and primitive streak formation. Subsequently, gastrulation does not take place. We note that the pattern of *Hcfc1*$^{epiKO/Y}$ lethality displays many similarities to loss of β-catenin function. These results reveal essential new roles for HCF-1 in early embryonic cell proliferation and development.

1. Introduction

In animals, early embryonic development is associated with rapid rounds of cell division, which allow the multicellular embryo to acquire cell numbers sufficient to support cell differentiation and development. These rapid rounds of cell division often short circuit cell-cycle regulators particularly of the G1 phase. Consequently, many G1-phase cell-cycle regulators such as transcriptional activators (e.g., E2Fs), repressors (Retinoblastoma protein (pRb) pocket-protein family), and repressors of repressors (e.g., cyclin–CDK complexes) are not required for early developmental events before embryonic day (E) 8.5, including gastrulation (reviewed in Ciemerych and Sicinski (2005)).

Here, we study a broadly active transcriptional co-regulator called HCF-1 encoded by the X-chromosome-linked *Hcfc1* gene in mice (Frattini et al., 1996; Kristie, 1997). HCF-1, in human a 2035 amino acid protein first identified as a host-cell factor for herpes simplex virus infection (reviewed by Wysocka and Herr (2003)), is required for the proliferation of cells in culture (Goto et al., 1997; Julien and Herr, 2003), at least in part, by its ability to associate with both DNA sequence-specific (e.g., E2F1 and E2F4, THAP11/Ronin, Myc) and chromatin-modifying (e.g., MLL and Set1 histone H3 lysine 4 methyltransferase, Sin3 histone deacetylase and BAP1 deubiquitinase) transcriptional regulators (reviewed by Zargar and Tyagi (2012); see also Thomas et al. (2015)). In culture, HCF-1 is required for both passage from G1 to S phase (Goto et al., 1997) and proper passage through M phase (Reilly and Herr, 2002); promotion of G1-to-S phase passage is linked to the ability of HCF-1 to associate with E2F proteins (Knez et al., 2006; Tyagi et al., 2007; Tyagi and Herr, 2009) and THAP11 (Parker et al., 2014).

We have recently described a conditional knock-out (cKO) mouse allele called *Hcfc1*^{lox}, where the presence of Cre recombinase induces deletion of two essential exons leading to the predicted synthesis of a small inactive truncated 66 amino acid HCF-1 peptide (Minocha et al., 2016). *Hcfc1* expression is ubiquitous in embryonic and extraembryonic tissues (Minocha et al., 2016). Because the *Hcfc1* gene resides on the X chromosome, female offspring carry two *Hcfc1* alleles of which one or the other is randomly inactivated at around E4.5–E5.5 (Clerc and Avner, 2011), whereas male offspring only possess one allele, which remains active throughout development. Epiblast-specific inactivation of the *Hcfc1*^{lox} allele (generating an *Hcfc1*^{epiKO} allele) by E5.5 does not reduce the viability of heterozygous females but is embryonic lethal in male embryos (Minocha et al., 2016). In the surviving

* Corresponding authors.
E-mail addresses: daniel.constam@epfl.ch (D.B. Constam), winship.herr@unil.ch (W. Herr).
[1] Present address: Institut Pasteur, 25-28 rue du Docteur Roux, Paris, France.
[2] Present address: Academia Sinica, 128 Academia Road, Taipei, Taiwan.

http://dx.doi.org/10.1016/j.ydbio.2016.08.008

heterozygous female embryos, HCF-1-deficient cells are progressively and by E8.5 entirely replaced by HCF-1-positive cells carrying the deleted *Hcfc1*^{epiKO} allele on the inactive X chromosome (Minocha et al., 2016).

The progressive loss of HCF-1-deficient cells in an environment in which half the cells remain positive for HCF-1 could be owing to cell competition if HCF-1-deficient cells cannot replicate as efficiently as their wild-type neighbors (Baillon and Basler, 2014). Such a cell-competition effect has been observed in the mouse epiblast as a result of variable levels of Myc oncoprotein (Claveria et al., 2013). Alternatively, HCF-1-deficient cells may simply fail to replicate. These two possibilities can be distinguished by examining the *Hcfc1*$^{epiKO/Y}$ male embryos where no potentially competing embryonic HCF-1-positive cells are present. If heterozygous *Hcfc1*$^{epiKO/+}$ female embryos eliminate HCF-1-deficient cells by cell competition, the absence of HCF-1-positive competing cells should rescue epiblast cell replication in *Hcfc1*$^{epiKO/Y}$ males at least transiently.

Here, by analyzing *Hcfc1*$^{epiKO/Y}$ male embryos, we describe the specific requirement for HCF-1 in early mouse embryonic development. Generation of the epiblast-specific *Hcfc1*^{epiKO} allele around E5.5 rapidly halts cell-proliferation, leading to developmental arrest by E6.5 prior to gastrulation. Thus, unlike the many aforementioned G1-phase cell-cycle regulators, which are not essential until after gastrulation, HCF-1 function is required for early embryonic development. Indeed, *Hcfc1*$^{epiKO/Y}$ embryonic cells exit the cell cycle earlier than in heterozygous *Hcfc1*$^{epiKO/+}$ female embryos, suggesting that loss of HCF-1-deficient cells in *Hcfc1*$^{epiKO/+}$ heterozygotes is not due to competition. Rather, in the *Hcfc1*$^{epiKO/+}$ heterozygotes, HCF-1-positive cells appear to support the proliferation of their HCF-1-deficient neighbors.

2. Materials and methods

2.1. Mice

All experimental studies have been performed in compliance with the EU and national legislation rules, as advised by the Lemanique Animal Facility Network (Resal), concerning ethical considerations of transportation, housing, strain maintenance, breeding and experimental use of animals.

Homozygous mice bearing the *Hcfc1* conditional (lox) allele are referred as *Hcfc1*$^{lox/lox}$ in this study (Minocha et al., 2016). The *Hcfc1*^{lox} allele contains two loxP sites, one in intron 1 and another in intron 3 that undergo recombination in the presence of Cre recombinase. This removes exon 2 and 3 to generate the conditional knockout (cKO) allele encoding a highly truncated 66 amino acids long HCF-1 protein.

Other strains used include wild-type *C57BL/6* mice and *C57BL/6* mice carrying the *Sox2Cre*^{tg} transgene (Hayashi et al., 2002).

Females and littermate males were housed four to five per cage at 23 °C, with a 12:12h light–dark cycle and ad libitum access to water and food. The day of finding the vaginal plug was assumed to be 0.5 days post-coitum.

2.2. DNA isolation and genotyping

For genotyping, genomic DNA was isolated from mouse ear tags for postnatal mice or entire conceptus for whole embryos as previously described (Truett et al., 2000). For paraffin-embedded embryo sections, DNA for genotyping was extracted by (i) preferential scraping of the epiblast region of 3–4 sections with a surgical blade, (ii) transferring the scraped sections into an eppendorf tube, and (iii) deparaffinizing and xylene removal as described (Minocha et al., 2016). Subsequent DNA extraction was done as described (Truett et al., 2000). Samples were used for PCR amplification with specific primer sets using the KAPA2G Fast HotStart Genotyping PCR Mix (cat no. KK5621). The annealing was done at 62 °C for 15 s with an extension at 72 °C for 10 s.

Primers for genotyping are listed below.

For HCF-1: p1 (5'-GGAGGAACATGAGCTTTAGG-3'), p2 (5'-CAATAGGCGAGTACCATCACAC-3'), and p3 (5'-GGGAAAGTAGACCCACTCTG-3') (Minocha et al., 2016).

For Cre: Sense (5'-AGGTGTAGAGAAGGCACTTAGC-3') and Antisense (5'-CTAATCGCCATCTTCCAGCAGG-3') (Le and Sauer, 2000).

For mouse Y chromosome: Sry-1 (5'-AACAACTGGGCTTTGCACATTG-3') and Sry-2 (5'-GTTTATCAGGGTTTCTCTCTAGC-3') (Steele-Perkins et al., 2005).

2.3. BrdU incorporation

To label embryonic cells during S phase, pregnant mice were injected intraperitoneally 5-bromo-2'-deoxyuridine (BrdU; BD Biosciences, cat. # 550891) to a final concentration of 50 mg/kg body weight, sacrificed 24h post-injection, and BrdU incorporation revealed by immunofluorescence staining (see below).

2.4. Tissue histology and immunohistochemistry

Intact E5.5 to E8.5 embryos were paraffin-embedded and sectioned within their decidua along a saggital axis to generate 4 μm thick sections using a microtome (MICROM HM325). The paraffin-embedded sections were prepared for hematoxylin and eosin (HE) staining, and immunohistochemical detection of proteins.

Paraffin-embedded sections were (i) deparaffinized in xylene, (ii) rehydrated through graded alcohol washes, (iii) rinsed twice with PBS, (iv) antigen revealed by heating in a 750 W microwave oven until boiling (approximately 10 min) in citrate buffer (10 mM, pH 6.0), (v) allowed to slowly cool down at 4 °C, (vi) washed twice with PBS, (vii) blocked for 30 min with 2% normal goat serum (NGS) (Sigma-Aldrich, cat. #G9023) in PBS at room temperature (RT), (viii) incubated with specific primary antibody diluted in 2% NGS overnight at 4 °C, (ix) washed thrice with PBS, (x) incubated with secondary antibody for 30 min in the dark at RT, (xi) washed thrice with PBS, (xii) counterstained with 4',6-diamidino-2-phenylindole (DAPI) (Sigma-Aldrich, CAS # 28,718-90-3), (xiii) washed twice with PBS, (xiv) embedded with Mowiol mounting medium (Sigma-Aldrich, CAS # 9002-89-5), and (xv) analyzed using an AxioImager M1 microscope with AxioCam MRm monochrome and AxioCam MRc color cameras (Carl Zeiss AG, Oberkochen, Germany). Images were processed using AxioVision 4.8.2 software (Carl Zeiss AG, Oberkochen, Germany).

Primary antibodies used were: rabbit anti-HCF-1 (1:1000, H12 (Wilson et al., 1993)), rat anti-Ki67 (1:60, eBioscience cat. # 41-5698), mouse anti-HNF4α (1:100, R&D Systems cat. # PP-H1415-00), rabbit anti-Histone H3 phospho Ser10 (1:100, Abcam cat. # ab5176), rat anti-BrdU (1:250, AbD Serotec cat. # OBT0030), and mouse β-catenin (1:50, BD Biosciences, cat. # 610153).

Secondary antibodies used were: Goat anti-rabbit Alexa 488 (1:400, Molecular Probes cat. # A11034), goat anti-mouse Alexa 568 (1:500, Molecular Probes cat. # A11019), goat anti-rabbit Alexa 568 (1:1000, Molecular Probes cat. # A21069), goat anti-mouse Alexa 488 (1:400, Molecular Probes cat. # A11029), and donkey anti-mouse Alexa 594 (1:500, Molecular Probes cat. # A11005).

2.5. TUNEL assay

Terminal deoxynucleotidyl transferase-mediated dUTP-biotin nick end labeling (TUNEL) was performed on paraffin-embedded embryo sections with the *in situ* cell death detection kit (Roche Applied Science, product # 11684795910), according to the

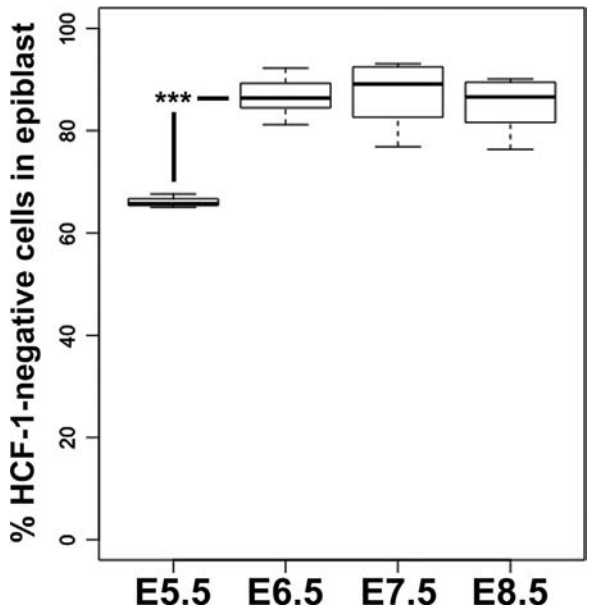

Fig. 1. Significant depletion of HCF-1-positive cells in the *Hcfc1*$^{epiKO/Y}$ male epiblasts by E6.5. Boxplot showing the percentage of HCF-1-negative cells in the epiblast of *Sox2Cre*^{tg} ; *Hcfc1*$^{epiKO/Y}$ male embryos from E5.5–E8.5 (E5.5 n=3; E6.5 n=6; E7.5 n=12; E8.5 n=5). The difference between the percentage of HCF-1-negative cells in epiblast of *Sox2Cre*^{tg} ; *Hcfc1*$^{epiKO/Y}$ male embryos at E5.5 and all other time points was highly significant (E5.5 versus E6.5 p-value 1.34×10^{-5}; E5.5 versus E7.5 p-value 3.45×10^{-8}; E5.5 versus E8.5 p-value 1.3×10^{-3}). The difference between the percentage of HCF-1-negative cells in the epiblast of *Sox2Cre*^{tg} ; *Hcfc1*$^{epiKO/Y}$ male embryos at E6.5, E7.5, and E8.5 was not significant (E6.5 versus E7.5 p-value 0.81; E7.5 versus E8.5 p-value 0.45).
Note: Data for the time point E5.5 shown in the boxplot has been reproduced from Minocha et al. (2016).

manufacturer's directions.

2.6. RNA whole mount in situ hybridization (wISH)

Whole-mount *in situ* hybridization (wISH) was performed as described using DIG-labeled antisense probes for the following genes: *Bmp4* (Jones et al., 1991), *Brachyury* (Wilkinson et al., 1990), *Hhex* (Bedford et al., 1993), *Cripto* (Ding et al., 1998), *Dkk1* (Glinka et al., 1998), *Fgf8* (Lee et al., 1997), *Lefty1* (Meno et al., 1997), *Nodal* (PCR-amplified exon 2) (Varlet et al., 1997), *Oct4* (Rosner et al., 1990), *Otx2* (Ang et al., 1994), and *Wnt3* (Roelink et al., 1990). Anti-DIG antibodies conjugated to alkaline phosphatase together with substrate BM purple (Roche Diagnostics) were used. Color reactions were developed until saturation at room temperature.

2.7. Quantitation and statistical analyses

For quantitation of the results shown in Figs. 1 and 6, cells in the epiblast region of single 4 μm-thick paraffin sections were counted. In Figs. 1, 2 and 6, the identification of the epiblast region was aided by co-staining with antibody against Oct4. The Student's *t*-test was performed by using the R package (www.r-project.org).

3. Results

To define the developmental steps that depend on HCF-1 in the epiblast, we crossed heterozygous *Sox2Cre* transgenic male mice (*Sox2Cre*^{tg}) (Hayashi et al., 2002) with homozygous *Hcfc1*$^{lox/lox}$ female mice and examined male embryos. The *Sox2Cre* transgene directs an onset of Cre recombinase synthesis around E4.5 exclusively in the post-implantation epiblast (Hayashi et al., 2002). The male *Hcfc1*$^{lox/Y}$ progeny lacking the *Sox2Cre*^{tg} express *Hcfc1* normally and possess a wild-type phenotype (Minocha et al., 2016), whereas in those carrying the *Sox2Cre*^{tg} allele the epiblast-specific epiKO allele is generated, leading to loss of anti-HCF-1 immunostaining in approximately 70% of epiblast cells by E5.5 (Minocha et al., 2016).

3.1. Epiblast-specific HCF-1 depletion leads to epiblast-specific developmental arrest by E6.5

As shown in Fig. 1, in *Sox2Cre*^{tg}; *Hcfc1*$^{epiKO/Y}$ embryos (heretofore referred to simply as *Hcfc1*$^{epiKO/Y}$), the percentage of HCF-1-deficient cells increases to 87% of epiblast cells by E6.5 and then varies between 85–90% of cells at E7.5 and E8.5. In contrast, the levels of HCF-1 in extraembryonic tissues, such as extraembryonic ectoderm (ExE) and visceral endoderm (VE), appeared unchanged (Fig. 2B3–B6). The major disappearance of HCF-1-positive epiblast cells at E6.5 was accompanied by a noticeable reduction in the size of the *Hcfc1*$^{epiKO/Y}$ epiblast relative to the corresponding extraembryonic tissue (Fig. 2E–G). Nevertheless, immunostaining of Oct4 revealed no overt change in epiblast fate at this stage (Fig. 3A–C, compare also Fig. 2A and B1).

At E7.5, the *Hcfc1*$^{epiKO/Y}$ epiblast, identified as Oct4 positive (Fig. 3D–F), did not increase in size compared to E6.5 (compare Fig. 2B1 and D1; Fig. 2F). The size of mutant epiblasts also did not noticeably increase at E8.5 (Supplemental Fig. 1A and B), indicating that their development is arrested at E6.5 and not simply delayed. At E9.5, *Hcfc1*$^{epiKO/Y}$ embryos were largely deformed and the epiblast region could not be identified easily (Supplemental Fig. 1C and D), probably owing to extensive embryonic cell death (see below).

In contrast to the epiblast, the ExE and VE of *Hcfc1*$^{epiKO/Y}$ embryos remained HCF-1-positive throughout the E6.5–E9.5 period (Fig. 2 and Supplemental Fig. 1). The ExE continued to grow until E8.5 despite the arrest of epiblast development, albeit less than in the *Hcfc1*$^{lox/Y}$ control littermates (compare Fig. 2C and D1, Fig. 2E and Supplemental Fig. 1B). In contrast, the embryonic VE (EmVE), which envelops *Hcfc1*$^{epiKO/Y}$ epiblasts, failed to grow and did not transition from a cuboidal to a simple squamous epithelial shape (VE arrowhead, Fig. 2D2) despite the continuous presence of nuclear HCF-1 (Fig. 2B5–B6 and D5–D6), suggesting a deficiency in epiblast-derived growth signals.

Altogether, these results demonstrate that HCF-1 is critical during early mouse embryonic development and that its epiblast-specific loss leads to a rapid growth arrest at E6.5 followed by cell non-autonomous secondary defects in extraembryonic lineages.

3.2. Loss of HCF-1 leads to cell-cycle exit around E6.5

The E5.5 to E7.5 phase of mouse development is characterized by rapid cell proliferation with doublings up to every 4–5 h (Snow, 1977) that largely skip the G1 phase and indeed lack elements of G1-phase regulation (see Introduction). HCF-1, like other G1-phase regulators, is essential for proper G1-phase progression in tissue-culture cells. In contrast, in *Hcfc1*$^{epiKO/+}$ females, HCF-1-deficient cells surrounded by HCF-1-positive cells continue proliferating at E6.5 and only disappear at a later stage owing to apoptosis (Minocha et al., 2016). We therefore asked here whether, in the absence of large numbers of surrounding HCF-1-positive cells, HCF-1-deficient cells exit the cell cycle and, if so, when.

Epiblast cells undergo multiple rounds of cell division both between E5.5 to E6.5 and between E6.5 to E7.5 (Snow, 1977). To reliably identify cells that have exited the cell cycle before these time windows, we measured the percentage of cells resistant to BrdU incorporation over a 24h labeling period (Fig. 4). We also identified replicating cells at E6.5 and E7.5 by histone H3

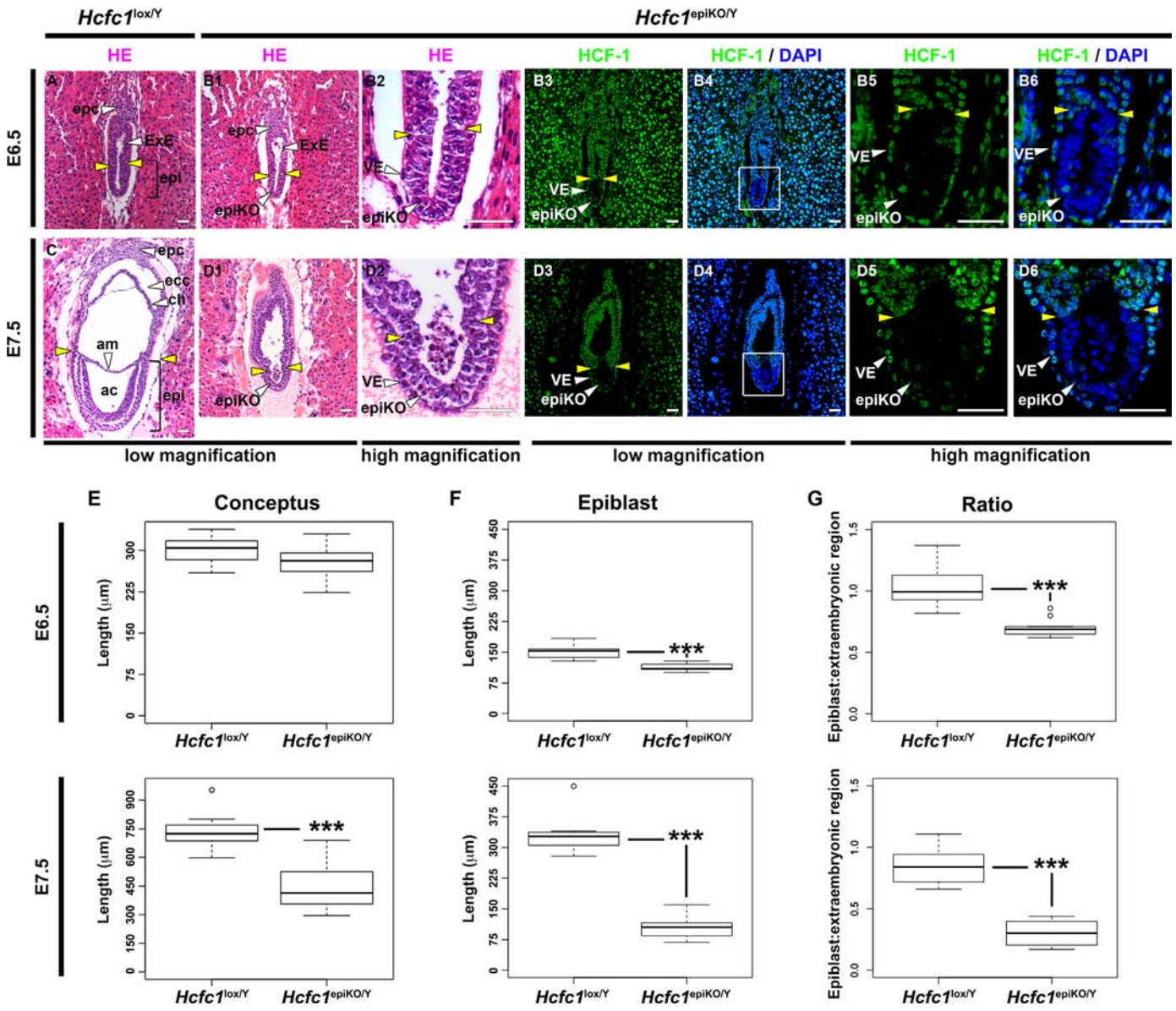

Fig. 2. Epiblast-specific depletion of HCF-1 leads to an embryonic developmental arrest at E6.5. HE staining on paraffin-embedded sections from (A and C) control *Hcfc1*$^{lox/Y}$ and (B1–B2 and D1–D2) *Sox2Cre*^{tg} ; *Hcfc1*$^{epiKO/Y}$ conditional knockout male embryos at (A, B1 and B2) E6.5 and (C, D1 and D2) E7.5. *Sox2Cre*^{tg} ; *Hcfc1*$^{epiKO/Y}$ male embryos at (B1) E6.5 and (D1) E7.5 are shown at higher magnification in subsequent panels B2 and D2, respectively. Adjacent paraffin-embedded sections of *Sox2Cre*^{tg} ; *Hcfc1*$^{epiKO/Y}$ male embryos (shown in B1–B2 and D1–D2) were taken for performing fluorescence staining with DAPI (blue) and anti-HCF-1 antibody (green) at (B3–B6) E6.5 and (D3–D6) E7.5. The boxed regions in (B4) E6.5 and (D4) E7.5 are shown at higher magnification in B5–B6 and D5–D6, respectively. The yellow arrowheads identify the boundary between extraembryonic and embryonic portions of the embryo. Quantifications of (E) conceptus length, (F) epiblast length, and (G) ratio of epiblast to extraembryonic (ExE) region were performed in control *Hcfc1*$^{lox/Y}$ (E6.5 n=9; E7.5 n=9) and *Sox2Cre*^{tg} ; *Hcfc1*$^{epiKO/Y}$ conditional knockout (E6.5 n=9; E7.5 n=12) male embryos at E6.5 and E7.5. The difference between conceptus length of *Hcfc1*$^{lox/Y}$ and *Sox2Cre*^{tg} ; *Hcfc1*$^{epiKO/Y}$ male embryos was not significant at E6.5 (p-value 0.11), and highly significant at E7.5 (p-value 8.8×10^{-6}). The difference between epiblast length of *Hcfc1*$^{lox/Y}$ and *Sox2Cre*^{tg} ; *Hcfc1*$^{epiKO/Y}$ male embryos was highly significant at both E6.5 (p-value 7.0×10^{-5}) and E7.5 (p-value 7.6×10^{-8}). The difference between ratio of epiblast to extraembryonic region of *Hcfc1*$^{lox/Y}$ and *Sox2Cre*^{tg} ; *Hcfc1*$^{epiKO/Y}$ male embryos was highly significant at both E6.5 (p-value 1.3×10^{-4}) and E7.5 (p-value 2.9×10^{-9}). ac, amniotic cavity; am, amnion; ch, chorion; ecc, ectoplacental cavity; epc, ectoplacental cone; epi, epiblast; epiKO, HCF-1-depleted epiblast; ExE, extraembryonic ectoderm; VE, visceral endoderm. Scale bar: 50 μm.

phosphoserine 10 (H3S10P) immunostaining of interphase and condensed mitotic chromosomes (Fig. 5). Identification of the epiblast region was aided by co-staining with Oct4 (Fig. 3). The results are quantitated in Fig. 6.

As expected, control E6.5 and E7.5 *Hcfc1*$^{lox/Y}$ embryos displayed considerable BrdU incorporation in both embryonic and extraembryonic cells (Fig. 4A and C). In contrast, *Hcfc1*$^{epiKO/Y}$ embryos displayed reduced BrdU incorporation in the embryonic lineage by 56% at E6.5 (Figs. 4A and B, and 6A) and by 77% at E7.5 (Fig. 4C and D, and Fig. 6A), suggesting a pronounced failure to enter S phase already by around E5.5, i.e. even before BrdU was injected for analysis at the E6.5 time point. Interestingly, compared to control *Hcfc1*$^{lox/Y}$ embryos, the BrdU labeling intensity was also reduced in the extraembryonic tissues (compare Fig. 4A2 with B2 and C2 with D2; see Supplemental Fig. 2 for quantitation), including the deciduum (see asterisk). The EmVE was particularly deficient in BrdU labeling in *Hcfc1*$^{epiKO/Y}$ embryos (compare Fig. 4A5 and B5; see Supplemental Fig. 2 for quantitation), consistent with a cell non-autonomous role for HCF-1 in the epiblast to maintain EmVE growth.

The H3S10P marker was readily detected both in embryonic and extraembryonic tissues in E6.5 and E7.5 *Hcfc1*$^{lox/Y}$ embryos (Fig. 5A4 and C4, magenta arrows). The number of H3S10P-labeled cells was, however, reduced in the *Hcfc1*$^{epiKO/Y}$ embryos compared

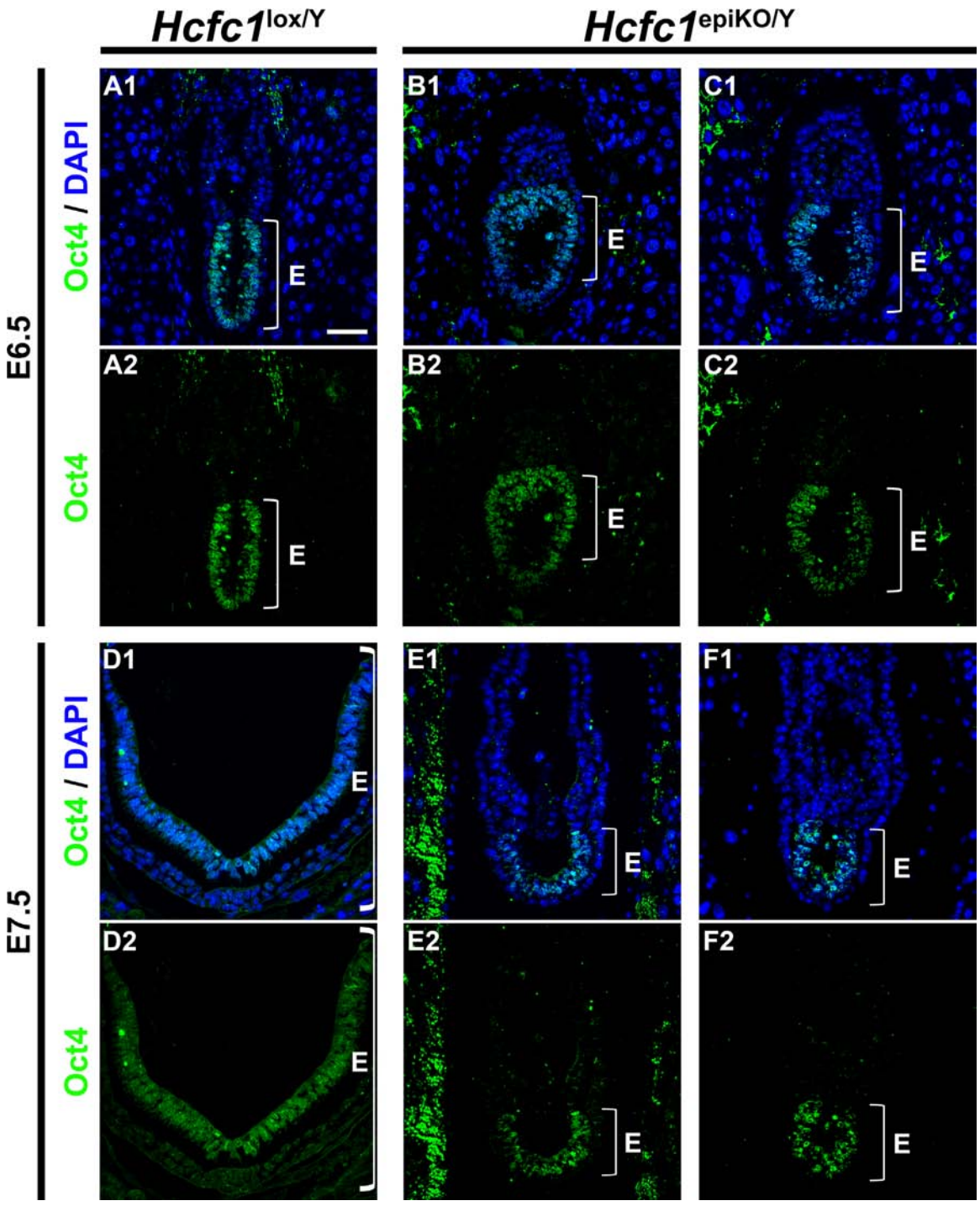

Fig. 3. Recognition of epiblast region in *Hcfc1*$^{epiKO/Y}$ embryos with antibody against Oct4. Immunofluorescence analysis of paraffin-embedded sections of (A and D) control *Hcfc1*$^{lox/Y}$ and (B, C, E, and F) *Sox2Cre*^{tg}; *Hcfc1*$^{epiKO/Y}$ male embryos with anti-Oct4 (green) and DAPI (blue) at (A, B, and C) E6.5 and (D, E, and F) E7.5. The brackets point to the epiblast (E) region. Scale bar: 50 μm.

to *Hcfc1*$^{lox/Y}$ embryos both at E6.5 (compare Fig. 5A and B; Fig. 6B) and E7.5 (compare Fig. 5C and D; Fig. 6B), in agreement with the reduced BrdU staining. Together, these results suggest that, although HCF-1-deficient cells display some proliferation, the large majority exits the cell cycle and arrests proliferation by E5.5–E7.5.

To examine the fate of HCF-1-deficient cells, we assayed for apoptotic cells in *Hcfc1*$^{epiKO/Y}$ embryos at E6.5 to E9.5 (Fig. 7 and Supplemental Fig. 3). In the epiblast, we observed an increase in the number of apoptotic cells in *Hcfc1*$^{epiKO/Y}$ embryos between E6.5 (8%) and E7.5 (27%) (Fig. 6C and Fig. 7B, D; magenta arrows). Interestingly, in five out of six embryos, we also observed apoptotic cells in the EmVE (Fig. 7D; light blue arrows). By E8.5 and E9.5, most cells stained positive for apoptosis (Supplemental Fig. 3B and D). Overall, these results suggest that the majority of the HCF-1-deficient cells exit the cell cycle around E6.5 and, after a delay, are eliminated via apoptosis.

3.3. Loss of HCF-1 in the epiblast impairs AVE formation and anterior-posterior (A-P) axis specification

Already before the widespread cell-cycle exit observed at E6.5, reciprocal signals between the epiblast and EmVE are essential to

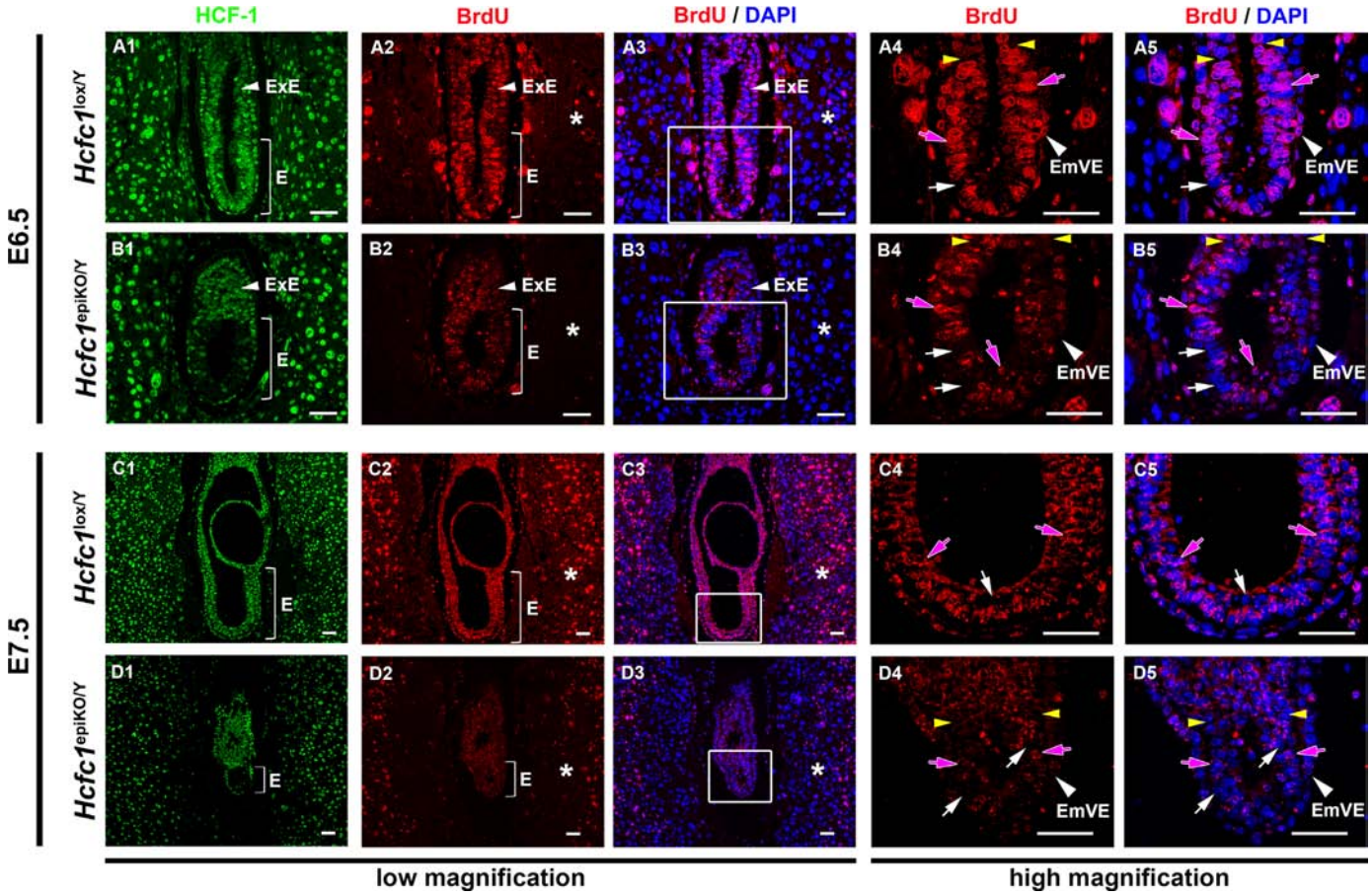

Fig. 4. Reduced number of proliferating cells in *Hcfc1*$^{epiKO/Y}$ epiblasts from E5.5 onwards. Immunofluorescence analysis of paraffin-embedded sections of (A and C) control *Hcfc1*$^{lox/Y}$ and (B and D) *Sox2Cre*^{tg} ; *Hcfc1*$^{epiKO/Y}$ male embryos at (A and B) E6.5 and (C and D) E7.5 after 24 h BrdU incorporation. Two consecutive paraffin-embedded sections were taken for (i) performing immunostaining with anti-HCF-1 antibody (green) and (ii) with S phase marker anti-BrdU (red) and DAPI (blue). The boxed regions in immunostained control (A3 and C3) *Hcfc1*$^{lox/Y}$ and (B3 and D3) *Sox2Cre*^{tg}; *Hcfc1*$^{epiKO/Y}$ male embryonic sections are shown at higher magnification in panels A4–A5 and C4–C5, and B4–B5 and D4–D5, respectively. The brackets point to the epiblast (E) region. The asterisk (*) denotes the decidua. The yellow arrowheads identify the boundary between extraembryonic and embryonic portions of the embryo. The magenta arrows point to BrdU-positive nuclei and white arrows point to BrdU-negative nuclei. EmVE, embryonic visceral endoderm; ExE, extraembryonic ectoderm. Scale bar: 50 μm.

specify anterior VE (AVE) and to pattern the future anterior-posterior (A-P) body axis. To test whether *Hcfc1* is required for A-P axis specification, we first monitored VE patterning by labeling the general VE marker HNF4α in *Hcfc1*$^{lox/Y}$ and *Hcfc1*$^{epiKO/Y}$ embryos. HNF4α levels began to decrease specifically in the EmVE at E5.5 both in *Hcfc1*$^{lox/Y}$ and *Hcfc1*$^{epiKO/Y}$ embryos and continued to do so in *Hcfc1*$^{lox/Y}$ controls until E6.5 as expected (Supplemental Fig. 4; Duncan et al., 1994; Morrisey et al., 1998). In *Hcfc1*$^{epiKO/Y}$ embryos, however, HNF4α failed to become restricted to the extraembryonic VE (ExVE) and HNF4α levels even increased ectopically throughout the VE by E7.5 (Fig. 8), indicating a marked defect in EmVE patterning.

To further investigate defects in EmVE patterning, we probed the expression of markers of AVE and A-P axis formation. Prior to E6.5, the distal-most cells of the EmVE (called DVE) normally migrate to the prospective anterior side of the egg cylinder ahead of future AVE cells that are accrued from nearby EmVE cells (Takaoka et al., 2011) and induced to express the genes encoding the homeodomain transcription factor Hhex (Beddington and Robertson, 1998, 1999; Thomas et al., 1998) and the TGFβ family member Lefty1 (Beddington and Robertson, 1998, 1999; Meno et al., 1997). A functional AVE and its proper migration are essential to specify and correctly position anterior cell fates in the adjacent epiblast (reviewed in Takaoka and Hamada (2012)).

Migrating DVE cells secrete the Wnt antagonist Dickkopf-1 (Dkk1), which may direct DVE migration by antagonizing the activity of the posterior determinant Wnt3 (Kimura-Yoshida et al., 2005). Although a *porcupine* mutant deficient in Wnt secretion and signaling did not show AVE migration defects (Biechele et al., 2013), we performed whole mount *in situ* hybridization (wISH) for *Dkk1* and for the AVE markers *Lefty1* and *Hhex* at E6.5 to visualize possible effects of HCF-1 loss on AVE formation (Fig. 9). While expression of *Dkk1* appeared normal in the *Hcfc1*$^{epiKO/Y}$ embryos (Fig. 9A, compare panels c and c'), *Lefty1*-expressing cells ectopically accumulated distally in E6.5 *Hcfc1*$^{epiKO/Y}$ embryos (Fig. 9A, a'). Moreover, *Hhex* expression, which normally marks both DVE and AVE was absent (Fig. 9A, panel b and b'). These results suggest that HCF-1 is required in the epiblast for AVE migration and normal EmVE patterning.

AVE migration and *Lefty-1* expression depend on Nodal and its coreceptor Cripto (Brennan et al., 2001; Ding et al., 1998; Kimura-Yoshida et al., 2005; Trichas et al., 2011; Yamamoto et al., 2004). To assess whether epiblast depletion of HCF-1 affects *Nodal* or *Cripto* expression, their corresponding mRNA levels were analyzed by wISH. *Nodal* and *Cripto* mRNAs were clearly present in the epiblast of both *Hcfc1*$^{lox/Y}$ and *Hcfc1*$^{epiKO/Y}$ embryos (Fig. 9A, panels d and d', and e and e'). In *Hcfc1*$^{epiKO/Y}$ embryos, however, they failed to become restricted to the posterior side (panels d' and e'), indicating a lack of A-P axis formation.

Graded *Nodal* expression along the A-P axis requires feedback regulation mediated by the mutual inhibition between *Otx2* and *Wnt3*: Induction of *Wnt3* in the posterior epiblast by Nodal and

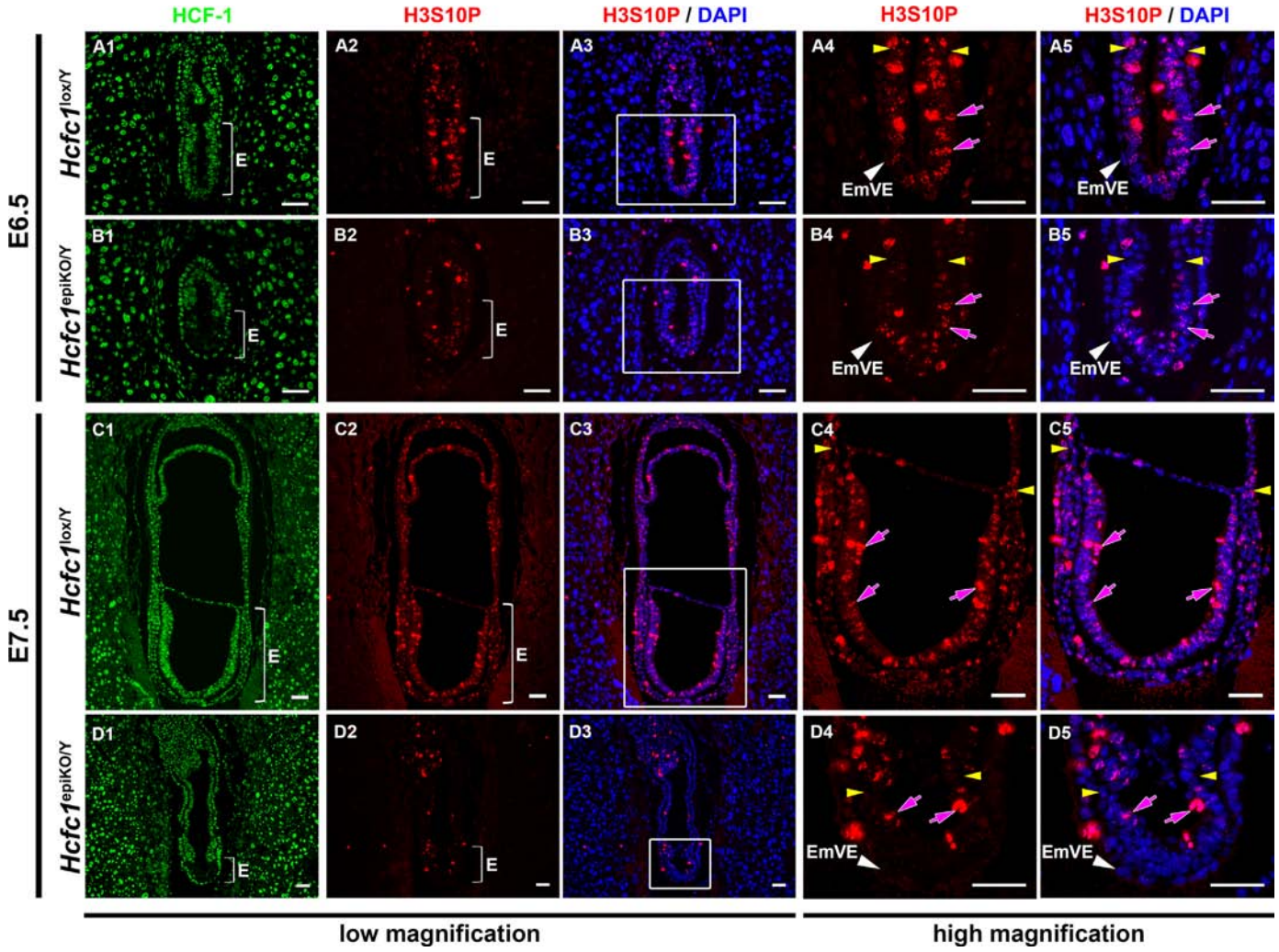

Fig. 5. Reduced H3S10P-positive cells in *Hcfc1*$^{epiKO/Y}$ epiblasts from E6.5 onwards. Immunofluorescence analysis of paraffin-embedded sections of (A and C) control *Hcfc1*$^{lox/Y}$ and (B and D) *Sox2Cre*^{tg} ; *Hcfc1*$^{epiKO/Y}$ male embryos at (A and B) E6.5 and (C and D) E7.5. Two consecutive paraffin-embedded sections were taken for performing immunostaining with (i) anti-HCF-1 antibody (green) and (ii) anti-H3S10P (red) and DAPI (blue). The boxed regions in immunostained control (A3 and C3) *Hcfc1*$^{lox/Y}$ and (B3 and D3) *Sox2Cre*^{tg} ; *Hcfc1*$^{epiKO/Y}$ male embryonic sections are shown at higher magnification in panels A4–A5 and C4–C5, and B4–B5 and D4–D5, respectively. The brackets point to the epiblast (E) region. The yellow arrowheads identify the boundary between extraembryonic and embryonic portions of the embryo. The magenta arrows point to H3S10P-positive nuclei and white arrows point to H3S10P-negative nuclei. EmVE, embryonic visceral endoderm. Scale bar: 50 μm.

possibly BMP4 inhibits *Otx2* expression (Beddington and Robertson, 1999; Ben-Haim et al., 2006; Lawson et al., 1999; Winnier et al., 1995), whereas upregulation of *Otx2* at the anterior pole induces AVE migration and thereby restricts Nodal and Wnt3 signaling to the posterior (Ang et al., 1994; Ding et al., 1998; Kimura et al., 2000; Kimura-Yoshida et al., 2005; Liu et al., 1999; Simeone et al., 1993; Trichas et al., 2011; Yamamoto et al., 2004). *Wnt3* was readily detected in both wild-type and *Hcfc1*$^{epiKO/Y}$ embryos, confirming that Nodal and Cripto were active. In *Hcfc1*$^{epiKO/Y}$ embryos, however, *Wnt3* mRNA failed to be enriched at the prospective posterior pole and instead ectopically accumulated throughout the proximal epiblast (Fig. 9A, panel f'). Consistent with this ectopic *Wnt3* expression, expression of *Otx2* mRNA was confined to distal epiblast and only maintained at reduced levels in *Hcfc1*$^{epiKO/Y}$ mutants. Furthermore, *Otx2* expression in the EmVE and its A-P polarity in the epiblast were lost (Fig. 9, panel g'). Altogether, these results indicate that proximal-distal patterning still occurs in *Hcfc1*$^{epiKO/Y}$ embryos but fails to be converted into a functional A-P axis at E6.5, probably owing to a defective anterior migration of the AVE.

3.4. Lack of AVE development and A-P axis formation is followed by a failure of primitive streak formation

Because *Hcfc1*$^{epiKO/Y}$ embryos lacked A-P axis polarity at E6.5, we asked whether subsequent primitive streak formation and gastrulation movements might be inhibited. To address this question, we performed wISH of genes expressed in the primitive streak at E7.5, including *Cripto*, *Wnt3* and *Otx2*. In addition, we monitored the expression of the general epiblast-specific marker *Oct4*. Even though the *Hcfc1*$^{epiKO/Y}$ embryos were deformed with only tiny epiblasts, *Oct4* remained normally expressed (Fig. 9B, compare panels e and e'). Consistent with the patterning defects observed at E6.5, however, the levels of *Cripto*, *Wnt3* and *Otx2* mRNAs appeared to be reduced, and their graded distribution which marks the A-P axis of wild-type E7.5 embryos was impaired (Fig. 9B, panels a–c').

Wnt3 and *Nodal* are critical for primitive streak formation (Conlon et al., 1994; Liu et al., 1999). To directly monitor primitive streak formation, we analyzed the expression of two of their downstream targets, *Brachyury* and *Fgf8* (Crossley and Martin, 1995; Inman and Downs, 2006). *Brachyury* and *Fgf8* mRNAs were

markedly decreased in *Hcfc1*$^{epiKO/Y}$ embryos (Fig. 9B, panels f' and g') compared to *Hcfc1*$^{lox/Y}$ littermate embryos (panels f and g).

Cells that emanate from the primitive streak to form definitive endoderm eventually intermingle with the overlying HNF4α-positive VE. Interestingly, immunostaining of HNF4α protein, which marks the extraembryonic yolk sac endoderm of wild-type E8.5 embryos (Duncan et al., 1994; see Supplemental Fig. 5A2–4), revealed persistent presence of ectopic HNF4α in EmVE of *Hcfc1*$^{epiKO/Y}$ mutants (see Supplemental Fig. 5B3). Besides confirming a defect in EmVE maturation, this result is consistent with a lack of germ layer formation.

Overall, these findings suggest that improper A-P axis formation leads to defective primitive streak formation upon loss of HCF-1 in the epiblast.

3.5. *Hcfc1*$^{epiKO/Y}$ *embryos display defective β-catenin activation*

β-catenin is a dual function protein that serves as both a nuclear transcriptional co-regulator and a regulator of cell–cell adhesion by associating with the plasma membrane. In β-catenin-dependent signaling, the transcriptional regulatory functions of β-catenin are activated by its release from an APC destruction complex in the cytoplasm followed by translocation to the nucleus where it associates with the TCF/LEF family of promoter-specific DNA-binding transcriptional regulators (Huelsken and Behrens, 2002).

As *Wnt3* was expressed but failed to induce primitive streak formation in *Hcfc1*$^{epiKO/Y}$ embryos, we asked whether the loss of HCF-1 affects β-catenin activation (i.e., nuclear localization). Immunostaining of *Hcfc1*$^{lox/Y}$ embryos between E6.5–7.5 stages readily detected β-catenin at the plasma membrane and nucleus of both embryonic and extraembryonic cells (Fig. 10; see also with DAPI co-staining in Supplemental Fig. 6; Mohamed et al., 2004). In contrast, *Hcfc1*$^{epiKO/Y}$ embryos displayed less intense overall β-catenin staining of plasma membrane and particularly of the nuclei (Fig. 10; see also Supplemental Fig. 6), indicating a possible effect on cell–cell adhesion but certainly a defect in the activation of β-catenin transcriptional regulatory functions.

4. Discussion

We have shown that epiblast-specific loss of HCF-1 in the early mouse embryo leads to a developmental arrest at E6.5 as well as cell non-autonomous effects on extraembryonic lineages. As a result, shortly after proximal-distal patterning, there is a failure of A-P axis specification and gastrulation possibly owing to reduced epiblast growth combined with impaired β-catenin-dependent signaling. We additionally found that HCF-1 plays a key role in the rapid cell proliferation phase of embryonic development around E6.5, a time when many other G1-phase regulators (e.g., E2Fs, Retinoblastoma pocket-protein family, cyclin–Cdk complexes) are not functional (see Introduction). These results contrast with those of loss of HCF-1 function in the worm *Caenorhabditis elegans*, where germ-line disruption of the *Ce hcf-1* gene is viable under normal growth conditions (Lee et al., 2007). It should be noted that an earlier embryonic-specific disruption of *Hcfc1* expression may well cause earlier developmental defects than those

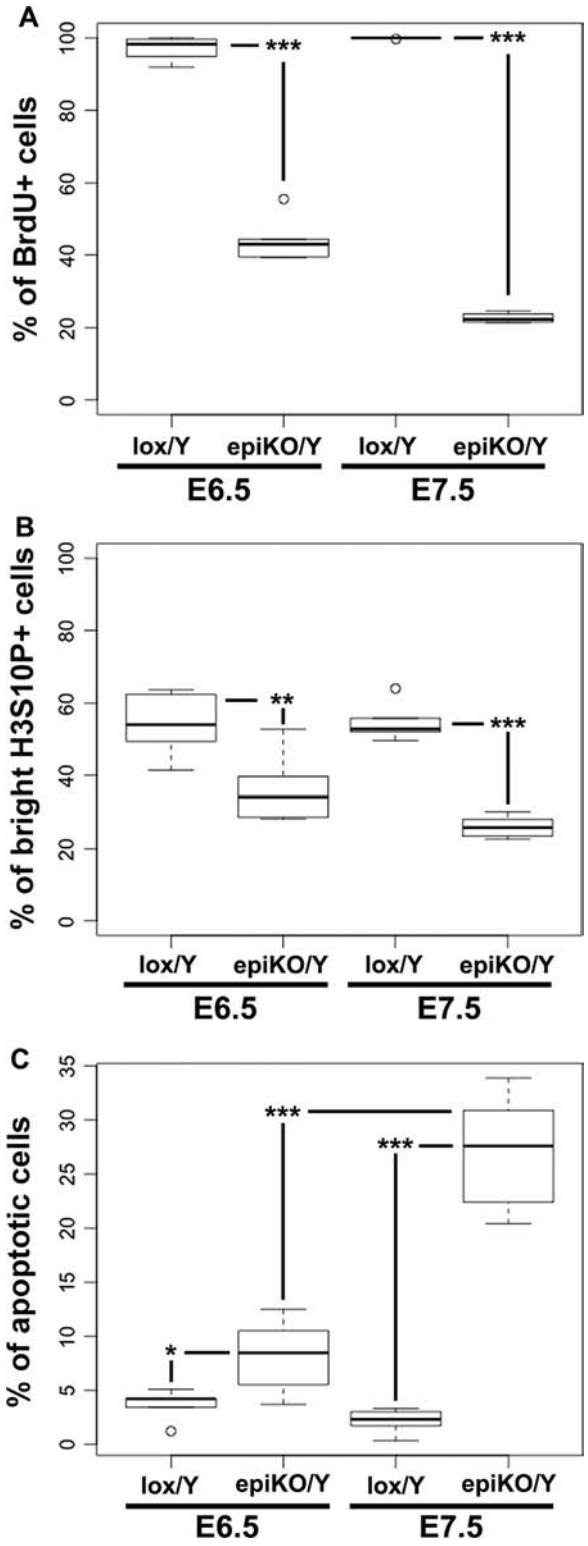

Fig. 6. An arrest in cell cycle is followed by increased apoptosis in *Hcfc1*$^{epiKO/Y}$ male embryos. Quantification of data presented in Figs. 4, 5 and 7. Boxplots showing the percentages of epiblast-specific cells positive for labeling for (A) BrdU, (B) H3S10P, or (C) TUNEL in sections of control *Hcfc1*$^{lox/Y}$ (labeled as lox/Y) and *Sox2Cre*^{tg} ; *Hcfc1*$^{epiKO/Y}$ (labeled as epiKO/Y) male embryos at E6.5 and E7.5. The difference between BrdU-positive epiblast cells of *Hcfc1*$^{lox/Y}$ (E6.5 n=7; E7.5 n=6) and *Sox2Cre*^{tg} ; *Hcfc1*$^{epiKO/Y}$ (E6.5n=6; E7.5 n=4) male embryos was highly significant at both E6.5 (p-value 7.0×10^{-8}) and E7.5 (p-value 1.8×10^{-6}). The difference between H3S10P-positive epiblast cells of *Hcfc1*$^{lox/Y}$ (E6.5 n=12; E7.5 n=5) and *Sox2Cre*^{tg} ; *Hcfc1*$^{epiKO/Y}$ (E6.5 n=6; E7.5 n=5) male embryos was highly significant at E6.5 (p-value 3.2×10^{-3}) and E7.5 (p-value 4.1×10^{-5}). The difference between TUNEL-positive epiblast cells of *Hcfc1*$^{lox/Y}$ (E6.5 n=6; E7.5 n=7) and *Sox2Cre*^{tg} ; *Hcfc1*$^{epiKO/Y}$ (E6.5 n=6; E7.5 n=5) male embryos was significant at E6.5 (p-value 0.02) and highly significant at E7.5 (p-value 5.0×10^{-4}). The difference between TUNEL-positive epiblast cells of E6.5 and E7.5 *Sox2Cre*^{tg} ; *Hcfc1*$^{epiKO/Y}$ male embryos was also highly significant (p-value 5.4×10^{-4}).

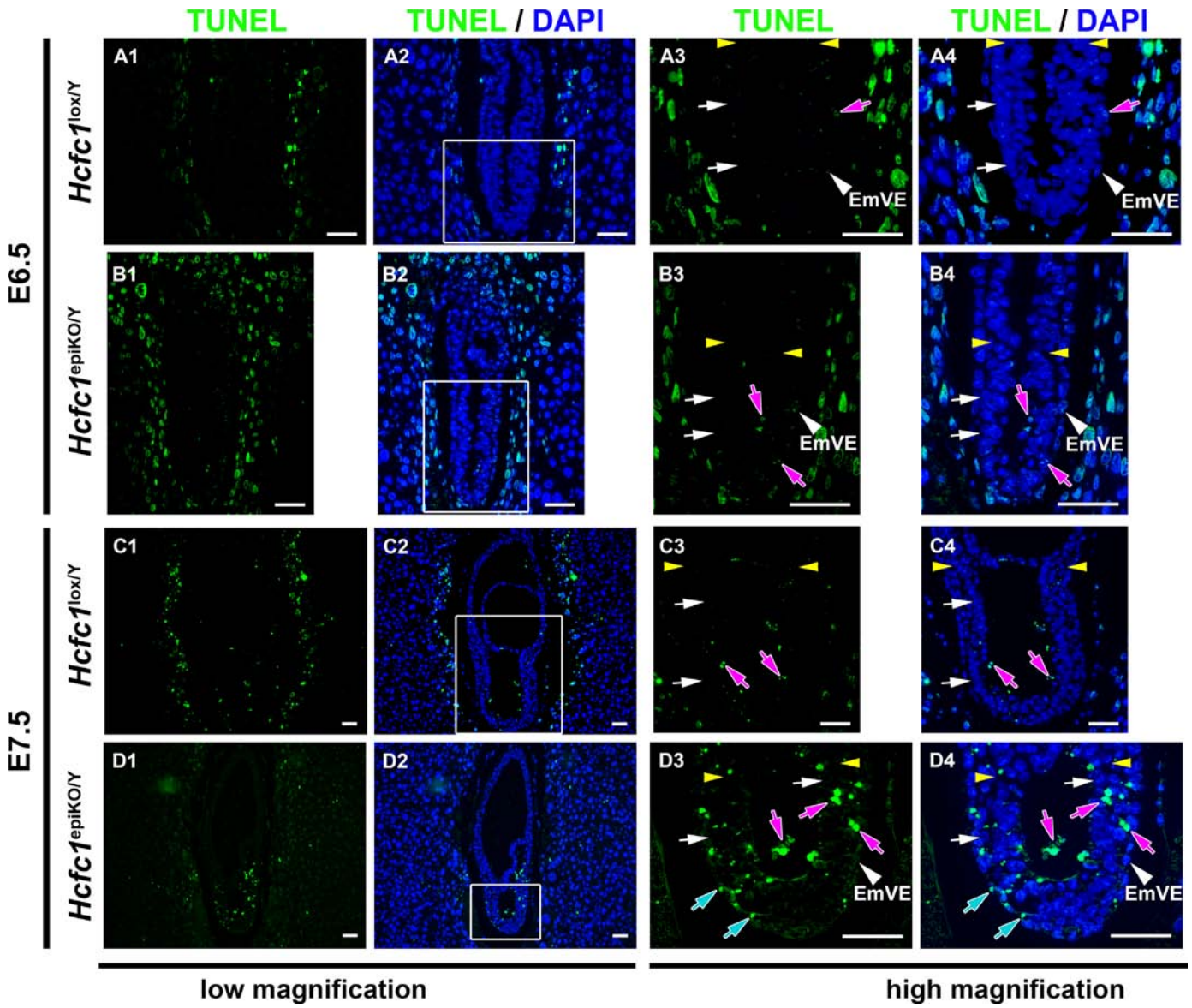

Fig. 7. Percentage of apoptotic cells significantly increases in *Hcfc1*$^{epiKO/Y}$ epiblasts by E7.5. TUNEL assay was performed on paraffin-embedded sections of (A and C) control *Hcfc1*$^{lox/Y}$ and (B and D) *Sox2Cre*^{tg} ; *Hcfc1*$^{epiKO/Y}$ male embryos co-stained with DAPI (blue) at (A and B) E6.5 and (C and D) E7.5. TUNEL-positive apoptotic cells are shown in green. The boxed regions in immunostained control (A2 and C2) *Hcfc1*$^{lox/Y}$ and (B2 and D2) *Sox2Cre*^{tg} ; *Hcfc1*$^{epiKO/Y}$ male embryonic sections are shown at higher magnification in subsequent panels in A3–A4 and C3–C4, and B3–B4 and D3–D4, respectively. The yellow arrowheads identify the boundary between extraembryonic and embryonic portions of the embryo. The magenta arrows point to TUNEL-positive nuclei and white arrows point to TUNEL-negative nuclei in the epiblast. The light blue arrows point to TUNEL-positive nuclei in the EmVE. Scale bar: 50 μm.

described here. Whether the case or not, the essential nature of HCF-1 for development has clearly varied significantly during metazoan evolution.

4.1. HCF-1 in early embryonic cell proliferation

As an X-linked gene, *Hcfc1* is randomly inactivated in the female mammalian embryo around E4.5–E5.5 (Clerc and Avner, 2011). In heterozygous *Hcfc1*$^{epiKO/+}$ female embryos, random X inactivation results in an approximately 50:50 mixture of HCF-1-positive and -deficient cells after which the HCF-1-deficient cells disappear (Minocha et al., 2016). To distinguish whether HCF-1-deficient cells are outgrown by competing HCF-1-positive cells, or instead simply fail to replicate, we here monitored cell proliferation in male *Hcfc1*$^{epiKO/Y}$ embryos. We observed widespread cell-cycle exit after E5.5 specifically in the mutant epiblasts, followed — after a delay — by apoptosis. This *Hcfc1*$^{epiKO/Y}$ cell-cycle exit is earlier than observed for HCF-1-deficient cells in *Hcfc1*$^{epiKO/+}$ heterozygotes (Minocha et al., 2016), suggesting that, in the *Hcfc1*$^{epiKO/+}$ heterozygous female embryos, HCF-1-positive cells help sustain the proliferation of their HCF-1-deficient neighbors. These results suggest a noncompetitive model for loss of HCF-1-deficient cells in *Hcfc1*$^{epiKO/+}$ heterozygous female embryos. Such cell non-autonomous cooperation may be important for the efficient survival observed of *Hcfc1*$^{epiKO/+}$ heterozygous female embryos (Minocha et al., 2016).

Despite essential roles of HCF-1 in cell proliferation and cell survival, the analysis of *Hcfc1*$^{epiKO/Y}$ mutants revealed significant residual epiblast growth between E5.5–E6.5 and no increase in apoptosis until later stages. Indeed, cell proliferation did not cease instantly after HCF-1 loss. A similar phenotype has been observed in the temperature-sensitive *Hcfc1* mutant hamster cell line tsBN67: When transferred to non-permissive temperature, tsBN67 cells continue the cell cycle for about two cell divisions before

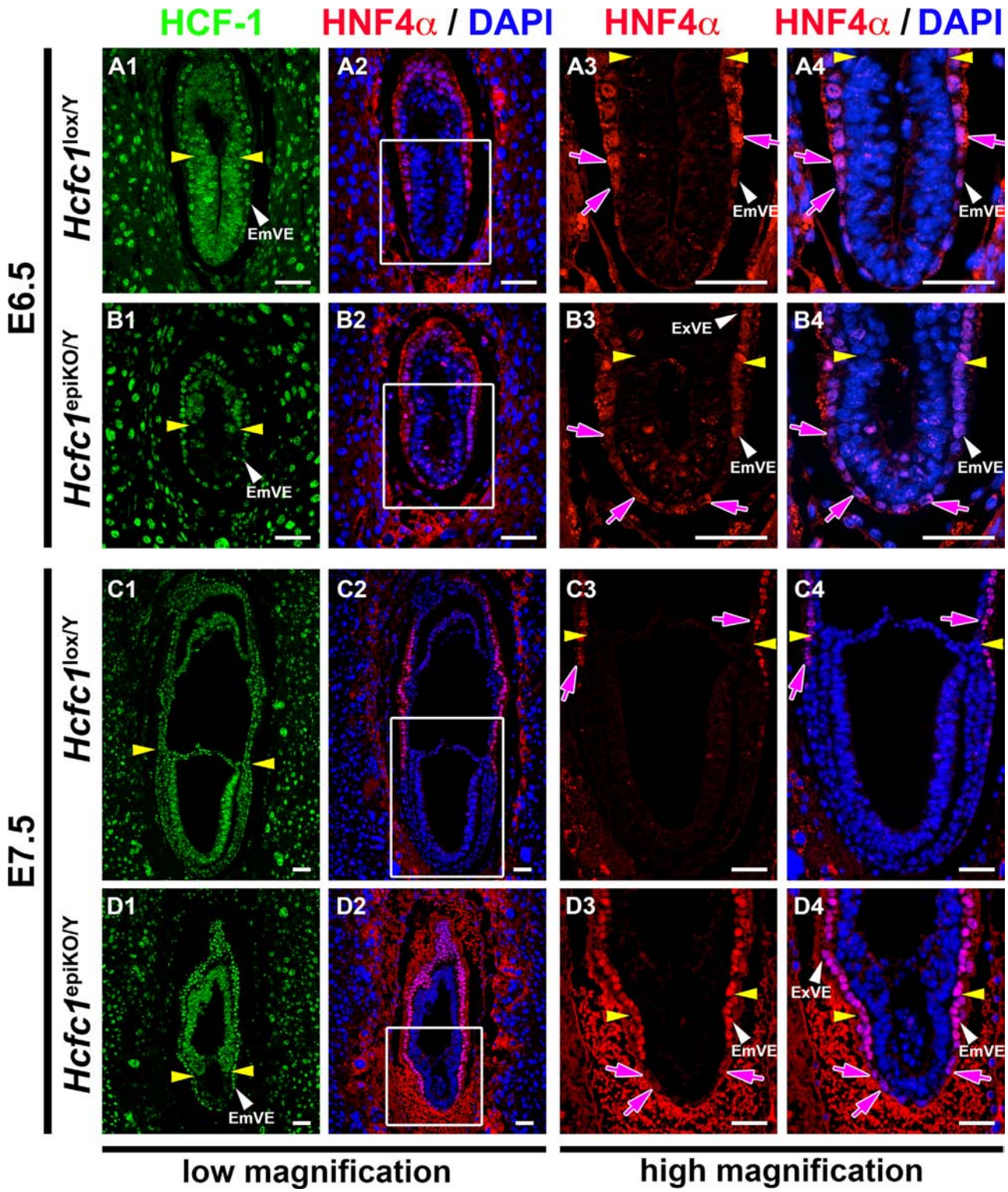

Fig. 8. Defective visceral endoderm patterning in *Hcfc1*$^{epiKO/Y}$ male embryos at E6.5 and E7.5. Immunofluorescence analysis of paraffin-embedded sections of (A and C) control *Hcfc1*$^{lox/Y}$ and (B and D) *Sox2Cre*^{tg} ; *Hcfc1*$^{epiKO/Y}$ male embryos at (A and B) E6.5 and (C and D) E7.5. Two consecutive paraffin-embedded sections were taken for immunostaining with (i) anti-HCF-1 antibody (green), and (ii) VE marker anti-HNF4α (red) and DAPI (blue). The boxed regions in (A2 and C2) control *Hcfc1*$^{lox/Y}$ and (B2 and D2) *Sox2Cre*^{tg} ; *Hcfc1*$^{epiKO/Y}$ male embryonic sections are shown at higher magnification in A3–A4 and C3–C4, and B3–B4 and D3–D4, respectively. The yellow arrowheads identify the boundary between extraembryonic and embryonic portions of the embryo. The magenta arrows point to HNF4α-positive nuclei. EmVE, embryonic visceral endoderm; ExVE, extraembryonic visceral endoderm. Scale bar: 50 μm.

entering a stable arrest in which there is little apoptosis (Goto et al., 1997; Reilly and Herr, 2002). In both tsBN67 and embryonic cells, cell-cycle arrest may be delayed for multiple reasons. For example, it may take time to deplete specific gene products that depend on HCF-1's function as a transcriptional regulator for synthesis. Additionally, the lack or delay of apoptosis in *Hcfc1*$^{epiKO/Y}$ cells after cell cycle exit may reflect an HCF-1 role in promoting apoptosis as described previously (Tyagi and Herr, 2009).

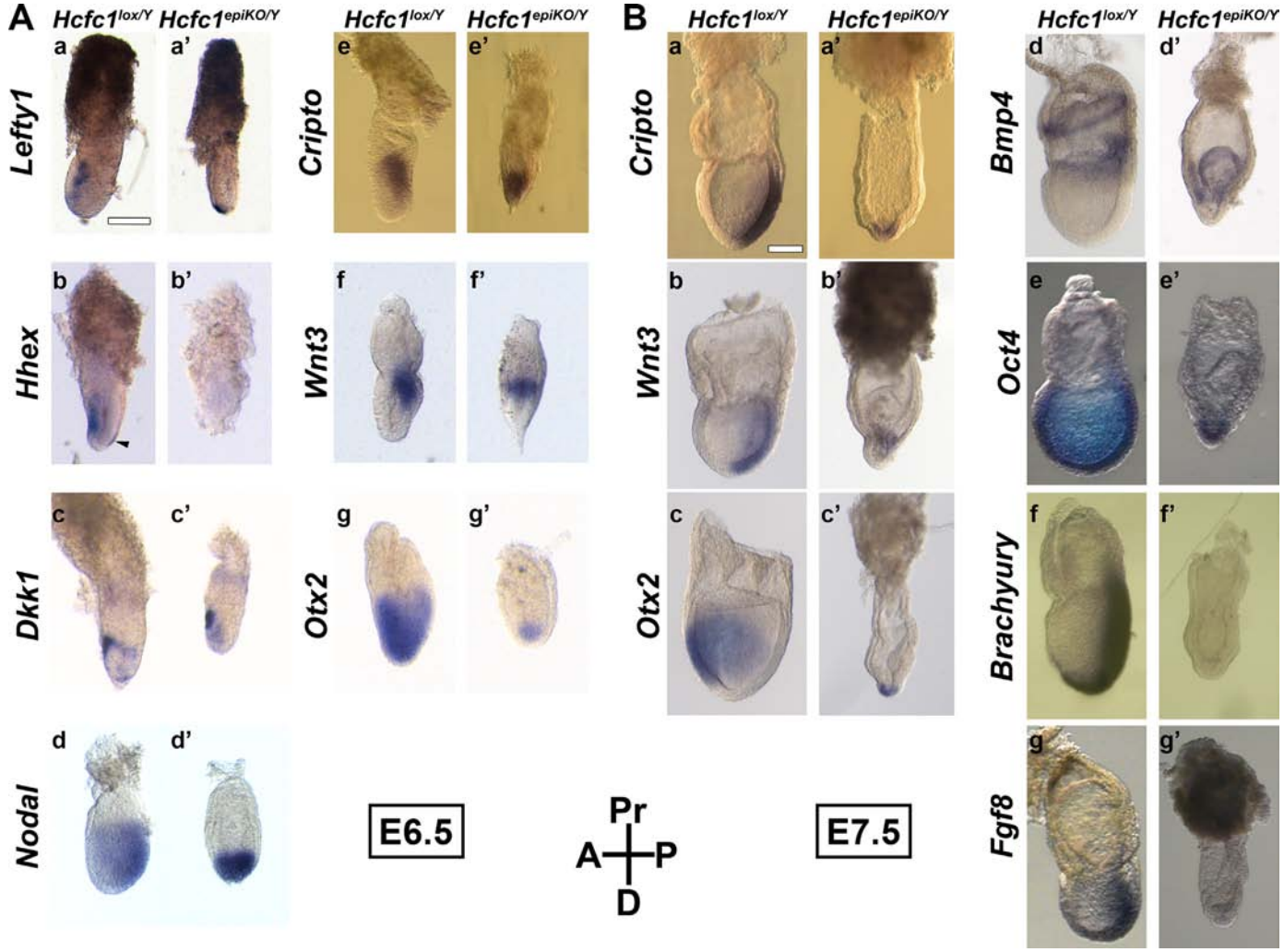

Fig. 9. Lack of AVE migration and primitive streak formation in *Hcfc1*$^{epiKO/Y}$ male embryos. (A) wISH analysis of (a and a') *Lefty1*, (b and b') *Hhex*, (c and c') *Dkk1*, (d and d') *Nodal*, (e and e') *Cripto*, (f and f') *Wnt3*, and (g and g') *Otx2* expression in (a, b, c, d, e, f, and g) control *Hcfc1*$^{lox/Y}$ and (a', b', c', d', e', f', and g') *Sox2Cre*^{tg} ; *Hcfc1*$^{epiKO/Y}$ male embryos at E6.5. The arrowhead in panel Ab points to the *Hhex* labeling in the emerging definitive endoderm. Scale bar shown in Aa: 130 μm for all panels at E6.5. (B) wISH analysis of (a and a') *Cripto*, (b and b') *Wnt3*, (c and c') *Otx2*, (d and d') *Bmp4*, (e and e') *Oct4*, (f and f') *Brachyury*, and (g and g') *Fgf8* expression in (a, b, c, d, e, f, and g) control *Hcfc1*$^{lox/Y}$ and (a', b', c', d', e', f', and g') *Sox2Cre*^{tg} ; *Hcfc1*$^{epiKO/Y}$ male embryos at E7.5. Scale bar shown in Ba: 140 μm for all panels at E7.5. The orientation of the embryos is as indicated: A, anterior; D, distal; Pr, proximal; P, posterior.

4.2. HCF-1 in early embryonic patterning

Upon epiblast-specific deletion of *Hcfc1* around E4.5–E5.5, there is a clear failure of A-P axis specification and subsequent gastrulation. The impaired cell proliferation after E6.5 in the *Hcfc1*$^{epiKO/Y}$ embryos may, at least in part, account for this phenotype since the presence of a certain number of epiblast cells and active cell proliferation are critical to initiate and sustain germ layer formation during gastrulation (reviewed in Tam and Behringer (1997)). Normal proliferation in the epiblast is also necessary for AVE formation during A-P axis specification (Stuckey et al., 2011). The number of epiblast cells increases approximately 4.5- to 5-fold (to around 660 cells) between E5.5 and E6.5 (Snow, 1977), which is important for gastrulation to initiate. The developmental arrest of *Hcfc1*$^{epiKO/Y}$ embryos just prior to gastrulation thus likely reflects their failure to attain the necessary threshold number of epiblast cells. According to a computational model, such a community effect may involve the enlargement of the pool of cells that produce Nodal since two kinetically distinct feedback loops that drive Nodal autoinduction cannot account for the elevated signaling thresholds that specify mesoderm and endoderm, except if the source of Nodal-producing cells increases substantially over time (Ben-Haim et al., 2006). In particular, the relatively early time of onset of *Wnt3* expression at around E6.0 in the epiblast, which is critically required downstream of *Nodal* to induce *Brachyury* expression in the primitive streak could not be explained by computational modeling without an epiblast cell community effect (Ben-Haim et al., 2006; Rivera-Perez and Magnuson, 2005; Tortelote et al., 2013).

Interestingly, we observed that *Hcfc1*$^{epiKO/Y}$ embryos, despite a noticeable size reduction, still induced *Wnt3* and yet failed to accumulate nuclear β-catenin on time at E6.5, or the Wnt/β-catenin transcriptional target *Brachyury* (Arnold et al., 2000). Since all Wnts rely on Porcupine function to signal through β-catenin-dependent or -independent pathways (Najdi et al., 2012) and both *Porcupine* and *Wnt3* mutant embryos display a proper DVE to AVE conversion (Biechele et al., 2013; Tortelote et al., 2013; Yoon et al., 2015) unlike *Hcfc1*$^{epiKO/Y}$ embryos, it appears that defects in *Hcfc1*$^{epiKO/Y}$ embryos are due to loss of a Porcupine/Wnt-independent function of β-catenin. Indeed, the *Hcfc1*$^{epiKO/Y}$ embryos strikingly resembled embryos lacking β-catenin in various respects (see Supplemental Table 1 for a detailed comparison): Both *Hcfc1*$^{epiKO/Y}$ and β-catenin mutant embryos show (i) embryonic lethality around E8.5, (ii) normal signs of proximal-distal

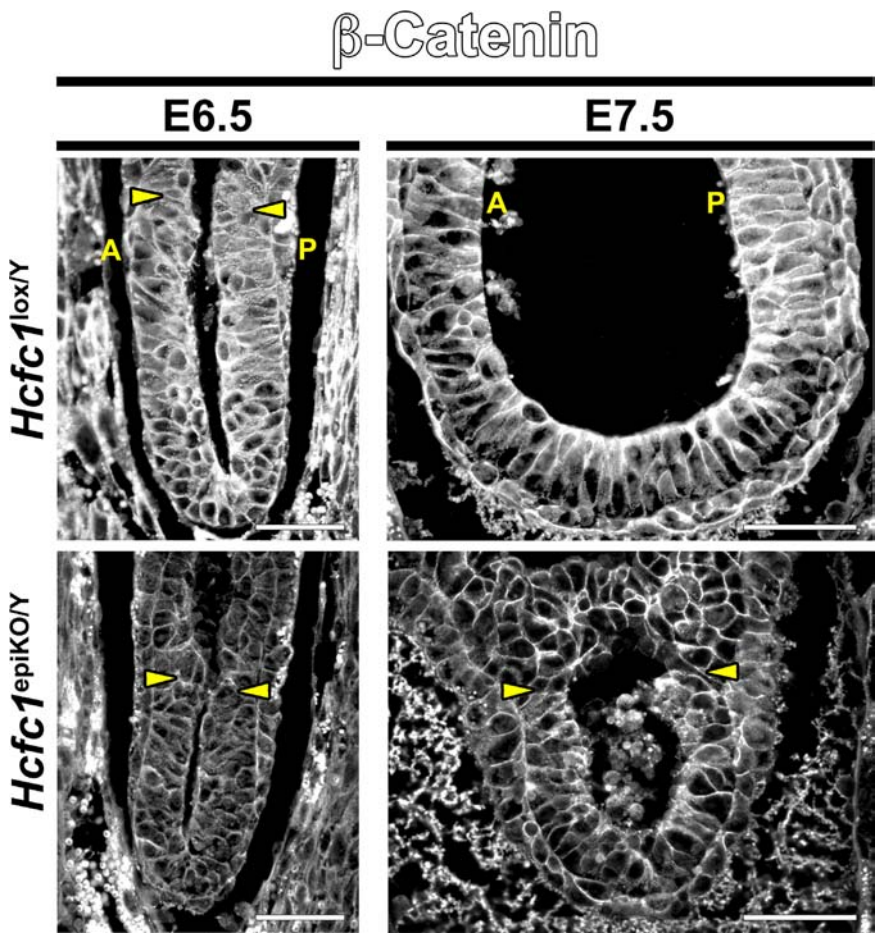

Fig. 10. Reduced levels of nuclear β-catenin in *Hcfc1*$^{epiKO/Y}$ male embryos. Immunofluorescence analysis of *Hcfc1*$^{lox/Y}$ and *Hcfc1*$^{epiKO/Y}$ male embryos stained with anti-β-catenin (white) at E6.5 and E7.5. The yellow arrowheads identify the boundary between extraembryonic and embryonic portions of the embryo. The β-catenin staining shown here in white is also shown in Supplemental Fig. 6 in red together with DAPI staining of nuclei. A, anterior; P, posterior. Scale bar: 50 μm.

patterning but defects in VE differentiation and A-P axis formation, and (iii) an absence of primitive streak formation and gastrulation (Haegel et al., 1995; Huelsken et al., 2000; Mohamed et al., 2004; Rudloff and Kemler, 2012).

These observations suggest a role for HCF-1 in β-catenin-dependent signaling. Such a role could be transcriptional. Indeed, HCF-1 associates with various transcription factors such as E2Fs, Ronin/Thap11, YY1, GABP, and ZNF143 to bind many promoters in mouse embryonic stem (ES) cells (743 promoters) and human HeLa cancer cells (5400 promoters), including promoters for components that regulate β-catenin stability (Dejosez et al., 2010; Michaud et al., 2013; Parker et al., 2014; Tyagi et al., 2007). Among the HCF-1-bound promoters in ES cells (Dejosez et al., 2010) are those for gene products that destabilize β-catenin (e.g., β-transducin repeat containing protein (Btrc) and F-box and WD-40 domain protein 11 (Fbxw11), which are both part of the SCF β-catenin degradation complex, and glycogen synthase kinase 3α (Gsk3α), which triggers destabilization of β-catenin through phosphorylation dependent mechanisms) and stabilize β-catenin (e.g., casein kinase 2β; Csnk2β). Thus, HCF-1 may activate or inhibit β-catenin signaling, depending on the context.

4.3. HCF-1 in non-autonomous cell signaling

At E6.5, the *Hcfc1*$^{epiKO/Y}$ embryos, displayed incomplete extraembryonic EmVE differentiation, suggesting non-autonomous cell effects of the epiblast-specific loss of HCF-1 on surrounding extraembryonic tissue, including absence of anteriorly located *Lefty1* and *Hhex* expression. Epiblast cells stimulate VE cell proliferation and patterning and the anterior movement of DVE cells at least in part by secreting Nodal (Yamamoto et al., 2004). Nodal may promote DVE migration by several mechanisms, including upregulation of its own proprotein convertase Furin (Mesnard et al., 2006) and of the paired-like homeobox transcription factor Otx2 (Kimura et al., 2000) in the VE and by stimulating the localization of dishevelled-2 (Dvl2) on VE cell membranes (Trichas et al., 2011). The downregulation of the Nodal target *Otx2* observed in the VE and in the epiblast of *Hcfc1*$^{epiKO/Y}$ embryos is consistent with the observed DVE cell migration defect (Kimura et al., 2000). However, as Nodal was able to induce *Lefty1* but not *Otx2* in the VE, epiblast-specific loss of HCF-1 might affect additional transcriptional activators upstream of *Otx2* such as Lhx1 or Foxa2 (Costello et al., 2015).

In conclusion, HCF-1 plays important roles in early embryonic cell proliferation and signaling events. Possessing such fundamental and essential functions in development may explain in part why it was targeted by herpes simplex virus as a key host-cell factor to coordinate its infection cycle.

Competing interest statement

The authors declare that they have no competing interests.

Author contributions

The experiments were conceived and designed by S.M., T.-L.S., D. C., and W.H. The experiments were performed by S.M., S.B., T.-L. S., and C.M. S.M., S.B., T.-L.S., D.C., and W.H. analyzed the data. S.M., D.C., and W.H. wrote the paper. S.M., S.B., T.-L.S., D.C., and W.H. participated in the discussion of the data and in production of the final version of the manuscript.

Acknowledgments

We thank Danièle Pinatel and Séverine Marguerite Urfer for technical assistance. This research was supported by Swiss National Science Foundation Grants 31003A_147104 to WH and 31003A_156452 to DBC, and by the University of Lausanne to WH.

Appendix A. Supplementary material

Supplementary data associated with this article can be found in the online version at doi:10.1016/j.ydbio.2016.08.008.

References

Ang, S.L., Conlon, R.A., Jin, O., Rossant, J., 1994. Positive and negative signals from mesoderm regulate the expression of mouse Otx2 in ectoderm explants. Development 120, 2979–2989.
Arnold, S.J., Stappert, J., Bauer, A., Kispert, A., Herrmann, B.G., Kemler, R., 2000. Brachyury is a target gene of the Wnt/beta-catenin signaling pathway. Mech. Dev. 91, 249–258.
Baillon, L., Basler, K., 2014. Reflections on cell competition. Semin. Cell Dev. Biol. 32, 137–144.
Beddington, R.S., Robertson, E.J., 1998. Anterior patterning in mouse. Trends Genet. 14, 277–284.
Beddington, R.S., Robertson, E.J., 1999. Axis development and early asymmetry in mammals. Cell 96, 195–209.
Bedford, F.K., Ashworth, A., Enver, T., Wiedemann, L.M., 1993. HEX: a novel homeobox gene expressed during haematopoiesis and conserved between mouse and human. Nucleic Acids Res. 21, 1245–1249.
Ben-Haim, N., Lu, C., Guzman-Ayala, M., Pescatore, L., Mesnard, D., Bischofberger, M., Naef, F., Robertson, E.J., Constam, D.B., 2006. The nodal precursor acting via activin receptors induces mesoderm by maintaining a source of its convertases and BMP4. Dev. Cell 11, 313–323.
Biechele, S., Cockburn, K., Lanner, F., Cox, B.J., Rossant, J., 2013. Porcn-dependent Wnt signaling is not required prior to mouse gastrulation. Development 140, 2961–2971.
Brennan, J., Lu, C.C., Norris, D.P., Rodriguez, T.A., Beddington, R.S., Robertson, E.J., 2001. Nodal signalling in the epiblast patterns the early mouse embryo. Nature 411, 965–969.
Ciemerych, M.A., Sicinski, P., 2005. Cell cycle in mouse development. Oncogene 24, 2877–2898.
Claveria, C., Giovinazzo, G., Sierra, R., Torres, M., 2013. Myc-driven endogenous cell competition in the early mammalian embryo. Nature 500, 39–44.
Clerc, P., Avner, P., 2011. New lessons from random X-chromosome inactivation in the mouse. J. Mol. Biol. 409, 62–69.
Conlon, F.L., Lyons, K.M., Takaesu, N., Barth, K.S., Kispert, A., Herrmann, B., Robertson, E.J., 1994. A primary requirement for nodal in the formation and maintenance of the primitive streak in the mouse. Development 120, 1919–1928.
Costello, I., Nowotschin, S., Sun, X., Mould, A.W., Hadjantonakis, A.K., Bikoff, E.K., Robertson, E.J., 2015. Lhx1 functions together with Otx2, Foxa2, and Ldb1 to govern anterior mesendoderm, node, and midline development. Genes Dev. 29, 2108–2122.
Crossley, P.H., Martin, G.R., 1995. The mouse Fgf8 gene encodes a family of polypeptides and is expressed in regions that direct outgrowth and patterning in the developing embryo. Development 121, 439–451.
Dejosez, M., Levine, S.S., Frampton, G.M., Whyte, W.A., Stratton, S.A., Barton, M.C., Gunaratne, P.H., Young, R.A., Zwaka, T.P., 2010. Ronin/Hcf-1 binds to a hyperconserved enhancer element and regulates genes involved in the growth of embryonic stem cells. Genes Dev. 24, 1479–1484.
Ding, J., Yang, L., Yan, Y.T., Chen, A., Desai, N., Wynshaw-Boris, A., Shen, M.M., 1998. Cripto is required for correct orientation of the anterior-posterior axis in the mouse embryo. Nature 395, 702–707.
Duncan, S.A., Manova, K., Chen, W.S., Hoodless, P., Weinstein, D.C., Bachvarova, R.F., Darnell Jr., J.E., 1994. Expression of transcription factor HNF-4 in the extraembryonic endoderm, gut, and nephrogenic tissue of the developing mouse embryo: HNF-4 is a marker for primary endoderm in the implanting blastocyst. Proc. Natl. Acad. Sci. USA 91, 7598–7602.
Frattini, A., Chatterjee, A., Faranda, S., Sacco, M.G., Villa, A., Herman, G.E., Vezzoni, P., 1996. The chromosome localization and the HCF repeats of the human host cell factor gene (HCFC1) are conserved in the mouse homologue. Genomics 32, 277–280.
Glinka, A., Wu, W., Delius, H., Monaghan, A.P., Blumenstock, C., Niehrs, C., 1998. Dickkopf-1 is a member of a new family of secreted proteins and functions in head induction. Nature 391, 357–362.
Goto, H., Motomura, S., Wilson, A.C., Freiman, R.N., Nakabeppu, Y., Fukushima, K., Fujishima, M., Herr, W., Nishimoto, T., 1997. A single-point mutation in HCF causes temperature-sensitive cell-cycle arrest and disrupts VP16 function. Genes Dev. 11, 726–737.
Haegel, H., Larue, L., Ohsugi, M., Fedorov, L., Herrenknecht, K., Kemler, R., 1995. Lack of beta-catenin affects mouse development at gastrulation. Development 121, 3529–3537.
Hayashi, S., Lewis, P., Pevny, L., McMahon, A.P., 2002. Efficient gene modulation in mouse epiblast using a Sox2Cre transgenic mouse strain. Mech. Dev. 119 (Suppl. 1), S97–S101.
Huelsken, J., Behrens, J., 2002. The Wnt signalling pathway. J. Cell Sci. 115, 3977–3978.
Huelsken, J., Vogel, R., Brinkmann, V., Erdmann, B., Birchmeier, C., Birchmeier, W., 2000. Requirement for beta-catenin in anterior-posterior axis formation in mice. J. Cell Biol. 148, 567–578.
Inman, K.E., Downs, K.M., 2006. Localization of Brachyury (T) in embryonic and extraembryonic tissues during mouse gastrulation. Gene Expr. Patterns 6, 783–793.
Jones, C.M., Lyons, K.M., Hogan, B.L., 1991. Involvement of Bone Morphogenetic Protein-4 (BMP-4) and Vgr-1 in morphogenesis and neurogenesis in the mouse. Development 111, 531–542.
Julien, E., Herr, W., 2003. Proteolytic processing is necessary to separate and ensure proper cell growth and cytokinesis functions of HCF-1. EMBO J. 22, 2360–2369.
Kimura, C., Yoshinaga, K., Tian, E., Suzuki, M., Aizawa, S., Matsuo, I., 2000. Visceral endoderm mediates forebrain development by suppressing posteriorizing signals. Dev. Biol. 225, 304–321.
Kimura-Yoshida, C., Nakano, H., Okamura, D., Nakao, K., Yonemura, S., Belo, J.A., Aizawa, S., Matsui, Y., Matsuo, I., 2005. Canonical Wnt signaling and its antagonist regulate anterior-posterior axis polarization by guiding cell migration in mouse visceral endoderm. Dev. Cell 9, 639–650.
Knez, J., Piluso, D., Bilan, P., Capone, J.P., 2006. Host cell factor-1 and E2F4 interact via multiple determinants in each protein. Mol. Cell. Biochem. 288, 79–90.
Kristie, T.M., 1997. The mouse homologue of the human transcription factor C1 (host cell factor). Conservation of forms and function. J. Biol. Chem. 272, 26749–26755.
Lawson, K.A., Dunn, N.R., Roelen, B.A., Zeinstra, L.M., Davis, A.M., Wright, C.V., Korving, J.P., Hogan, B.L., 1999. Bmp4 is required for the generation of primordial germ cells in the mouse embryo. Genes Dev. 13, 424–436.
Le, Y., Sauer, B., 2000. Conditional gene knockout using cre recombinase. Methods Mol. Biol. 136, 477–485.
Lee, S., Horn, V., Julien, E., Liu, Y., Wysocka, J., Bowerman, B., Hengartner, M.O., Herr, W., 2007. Epigenetic regulation of histone H3 serine 10 phosphorylation status by HCF-1 proteins in *C. elegans* and mammalian cells. PloS One 2, e1213.
Lee, S.M., Danielian, P.S., Fritzsch, B., McMahon, A.P., 1997. Evidence that FGF8 signalling from the midbrain-hindbrain junction regulates growth and polarity in the developing midbrain. Development 124, 959–969.
Liu, P., Wakamiya, M., Shea, M.J., Albrecht, U., Behringer, R.R., Bradley, A., 1999. Requirement for Wnt3 in vertebrate axis formation. Nat. Genet. 22, 361–365.
Meno, C., Ito, Y., Saijoh, Y., Matsuda, Y., Tashiro, K., Kuhara, S., Hamada, H., 1997. Two closely-related left-right asymmetrically expressed genes, lefty-1 and lefty-2: their distinct expression domains, chromosomal linkage and direct neuralizing activity in Xenopus embryos. Genes Cells: Devoted Mol. Cell. Mech. 2, 513–524.
Mesnard, D., Guzman-Ayala, M., Constam, D.B., 2006. Nodal specifies embryonic visceral endoderm and sustains pluripotent cells in the epiblast before overt axial patterning. Development 133, 2497–2505.
Michaud, J., Praz, V., James Faresse, N., Jnbaptiste, C.K., Tyagi, S., Schutz, F., Herr, W., 2013. HCFC1 is a common component of active human CpG-island promoters and coincides with ZNF143, THAP11, YY1, and GABP transcription factor occupancy. Genome Res. 23, 907–916.
Minocha, S., Sung, T.L., Villeneuve, D., Lammers, F., Herr, W., 2016. Compensatory embryonic response to allele-specific inactivation of the murine X-linked gene Hcfc1. Dev. Biol. 412, 1–17.
Mohamed, O.A., Clarke, H.J., Dufort, D., 2004. Beta-catenin signaling marks the prospective site of primitive streak formation in the mouse embryo. Dev. Dyn. 231, 416–424.
Morrisey, E.E., Tang, Z., Sigrist, K., Lu, M.M., Jiang, F., Ip, H.S., Parmacek, M.S., 1998. GATA6 regulates HNF4 and is required for differentiation of visceral endoderm in the mouse embryo. Genes Dev. 12, 3579–3590.
Najdi, R., Proffitt, K., Sprowl, S., Kaur, S., Yu, J., Covey, T.M., Virshup, D.M., Waterman, M.L., 2012. A uniform human Wnt expression library reveals a shared secretory pathway and unique signaling activities. Differ. Res. Biol. Divers. 84, 203–213.
Parker, J.B., Yin, H., Vinckevicius, A., Chakravarti, D., 2014. Host cell factor-1 recruitment to E2F-bound and cell-cycle-control genes is mediated by THAP11 and ZNF143. Cell Rep. 9, 967–982.
Reilly, P.T., Herr, W., 2002. Spontaneous reversion of tsBN67 cell proliferation and cytokinesis defects in the absence of HCF-1 function. Exp. Cell Res. 277,

119–130.
Rivera-Perez, J.A., Magnuson, T., 2005. Primitive streak formation in mice is preceded by localized activation of Brachyury and Wnt3. Dev. Biol. 288, 363–371.
Roelink, H., Wagenaar, E., Lopes da Silva, S., Nusse, R., 1990. Wnt-3, a gene activated by proviral insertion in mouse mammary tumors, is homologous to int-1/Wnt-1 and is normally expressed in mouse embryos and adult brain. Proc. Natl. Acad. Sci. USA 87, 4519–4523.
Rosner, M.H., Vigano, M.A., Ozato, K., Timmons, P.M., Poirier, F., Rigby, P.W., Staudt, L.M., 1990. A POU-domain transcription factor in early stem cells and germ cells of the mammalian embryo. Nature 345, 686–692.
Rudloff, S., Kemler, R., 2012. Differential requirements for beta-catenin during mouse development. Development 139, 3711–3721.
Simeone, A., Acampora, D., Mallamaci, A., Stornaiuolo, A., D'Apice, M.R., Nigro, V., Boncinelli, E., 1993. A vertebrate gene related to orthodenticle contains a homeodomain of the bicoid class and demarcates anterior neuroectoderm in the gastrulating mouse embryo. EMBO J. 12, 2735–2747.
Snow, M.H.L., 1977. Gastrulation in the mouse: growth and regionalization of the epiblast. Development 42, 293–303.
Steele-Perkins, G., Plachez, C., Butz, K.G., Yang, G., Bachurski, C.J., Kinsman, S.L., Litwack, E.D., Richards, L.J., Gronostajski, R.M., 2005. The transcription factor gene Nfib is essential for both lung maturation and brain development. Mol. Cell. Biol. 25, 685–698.
Stuckey, D.W., Clements, M., Di-Gregorio, A., Senner, C.E., Le Tissier, P., Srinivas, S., Rodriguez, T.A., 2011. Coordination of cell proliferation and anterior-posterior axis establishment in the mouse embryo. Development 138, 1521–1530.
Takaoka, K., Hamada, H., 2012. Cell fate decisions and axis determination in the early mouse embryo. Development 139, 3–14.
Takaoka, K., Yamamoto, M., Hamada, H., 2011. Origin and role of distal visceral endoderm, a group of cells that determines anterior-posterior polarity of the mouse embryo. Nat. Cell Biol. 13, 743–752.
Tam, P.P., Behringer, R.R., 1997. Mouse gastrulation: the formation of a mammalian body plan. Mech. Dev. 68, 3–25.
Thomas, L.R., Foshage, A.M., Weissmiller, A.M., Popay, T.M., Grieb, B.C., Qualls, S.J., Ng, V., Carboneau, B., Lorey, S., Eischen, C.M., Tansey, W.P., 2015. Interaction of MYC with host cell factor-1 is mediated by the evolutionarily conserved Myc box IV motif. Oncogene.
Thomas, P.Q., Brown, A., Beddington, R.S., 1998. Hex: a homeobox gene revealing peri-implantation asymmetry in the mouse embryo and an early transient marker of endothelial cell precursors. Development 125, 85–94.
Tortelote, G.G., Hernandez-Hernandez, J.M., Quaresma, A.J., Nickerson, J.A., Imbalzano, A.N., Rivera-Perez, J.A., 2013. Wnt3 function in the epiblast is required for the maintenance but not the initiation of gastrulation in mice. Dev. Biol. 374, 164–173.
Trichas, G., Joyce, B., Crompton, L.A., Wilkins, V., Clements, M., Tada, M., Rodriguez, T.A., Srinivas, S., 2011. Nodal dependent differential localisation of dishevelled-2 demarcates regions of differing cell behaviour in the visceral endoderm. PLoS Biol. 9, e1001019.
Truett, G.E., Heeger, P., Mynatt, R.L., Truett, A.A., Walker, J.A., Warman, M.L., 2000. Preparation of PCR-quality mouse genomic DNA with hot sodium hydroxide and tris (HotSHOT). BioTechniques 29 (52), 54.
Tyagi, S., Herr, W., 2009. E2F1 mediates DNA damage and apoptosis through HCF-1 and the MLL family of histone methyltransferases. EMBO J. 28, 3185–3195.
Tyagi, S., Chabes, A.L., Wysocka, J., Herr, W., 2007. E2F activation of S phase promoters via association with HCF-1 and the MLL family of histone H3K4 methyltransferases. Mol. Cell 27, 107–119.
Varlet, I., Collignon, J., Robertson, E.J., 1997. nodal expression in the primitive endoderm is required for specification of the anterior axis during mouse gastrulation. Development 124, 1033–1044.
Wilkinson, D.G., Bhatt, S., Herrmann, B.G., 1990. Expression pattern of the mouse T gene and its role in mesoderm formation. Nature 343, 657–659.
Wilson, A.C., LaMarco, K., Peterson, M.G., Herr, W., 1993. The VP16 accessory protein HCF is a family of polypeptides processed from a large precursor protein. Cell 74, 115–125.
Winnier, G., Blessing, M., Labosky, P.A., Hogan, B.L., 1995. Bone morphogenetic protein-4 is required for mesoderm formation and patterning in the mouse. Genes Dev. 9, 2105–2116.
Wysocka, J., Herr, W., 2003. The herpes simplex virus VP16-induced complex: the makings of a regulatory switch. Trends Biochem. Sci. 28, 294–304.
Yamamoto, M., Saijoh, Y., Perea-Gomez, A., Shawlot, W., Behringer, R.R., Ang, S.L., Hamada, H., Meno, C., 2004. Nodal antagonists regulate formation of the anteroposterior axis of the mouse embryo. Nature 428, 387–392.
Yoon, Y., Huang, T., Tortelote, G.G., Wakamiya, M., Hadjantonakis, A.K., Behringer, R. R., Rivera-Perez, J.A., 2015. Extra-embryonic Wnt3 regulates the establishment of the primitive streak in mice. Dev. Biol. 403, 80–88.
Zargar, Z., Tyagi, S., 2012. Role of host cell factor-1 in cell cycle regulation. Transcription 3, 187–192.